Article scientifique    Article    2009       Published version       Open Access

# Transmembrane Signaling in the Maltose ABC Transporter MalFGK$_2$-E : PERIPLASMIC MalF-P2 LOOP COMMUNICATES SUBSTRATE AVAILABILITY TO THE ATP-BOUND MalK DIMER

Grote, Mathias; Polyhach, Yevhen; Jeschke, Gunnar; Steinhoff, Heinz-Jürgen; Schneider, Erwin; Bordignon, Enrica

### How to cite

# Transmembrane Signaling in the Maltose ABC Transporter MalFGK₂-E

## PERIPLASMIC MalF-P2 LOOP COMMUNICATES SUBSTRATE AVAILABILITY TO THE ATP-BOUND MalK DIMER*[S]

**Mathias Grote**[‡], **Yevhen Polyhach**[§], **Gunnar Jeschke**[§], **Heinz-Jürgen Steinhoff**[¶], **Erwin Schneider**[‡1], **and Enrica Bordignon**[§2]

*From the* [‡]*Institut für Biologie/Bakterienphysiologie, Humboldt Universität zu Berlin, Chausseestrasse 117, D-10115 Berlin, Germany,* [§]*ETH Zurich, Laboratory for Physical Chemistry, Wolfgang-Pauli-Strasse 10, 8093 Zurich, Switzerland, and* [¶]*Fachbereich Physik, Universität Osnabrück, Barbarastrasse 7, D-49076 Osnabrück, Germany*

ABC transporters are ubiquitous membrane proteins that translocate solutes across biological membranes at the expense of ATP. In prokaryotic ABC importers, the extracytoplasmic anchoring of the substrate-binding protein (receptor) is emerging as a key determinant for the structural rearrangements in the cytoplasmically exposed ATP-binding cassette domains and in the transmembrane gates during the nucleotide cycle. Here the molecular mechanism of such signaling events was addressed by electron paramagnetic resonance spectroscopy of spin-labeled ATP-binding cassette maltose transporter variants (MalFGK₂-E). A series of doubly spin-labeled mutants in the MalF-P2 domain involving positions 92, 205, 239, 252, and 273 and one triple mutant labeled at positions 205/252 in P2 and 83 in the Q-loop of MalK were assayed. The EPR data revealed that the substrate-binding protein MalE is bound to the transporter throughout the transport cycle. Concomitantly with the three conformations of the ATP-binding cassette MalK₂, three functionally relevant conformations are found also in the periplasmic MalF-P2 loop, strictly dependent on cytoplasmic nucleotide binding and periplasmic docking of liganded MalE to MalFG. The reciprocal communication across the membrane unveiled here gives first insights into the stimulatory effect of MalE on the ATPase activity, and it is suggested to be an important mechanistic feature of receptor-coupled ABC transporters.

ABC transporters form a large, ATP-dependent family of primary transporters, which can be found in all three kingdoms of life, and are involved in many vitally important transport processes across biological membranes. In bacteria, they represent 2% of all gene products. In humans, ~50% of all ABC transporter genes are involved in diseases, including the most frequent lethal inherited disease, cystic fibrosis (1). The spectrum of substrates ranges from small inorganic ions such as chloride to intact proteins. ABC transporters display a modular architecture composed of two nucleotide-binding domains (NBDs)[3] that contain all conserved sequence motifs and two transmembrane domains (TMDs), which can be arranged in any possible combination. Canonical ABC import systems, thus far confined to prokaryotes, require a fifth module for functionality, the extracytoplasmic substrate-binding protein or receptor. Binding protein-dependent ABC transporters mediate the uptake of a large variety of nutrients such as carbohydrates, amino acids, or peptides but are also involved in diverse physiological processes, including bacterial pathogenesis. For example, ABC importers that supply bacterial cells with essential iron ions (2) or transport signaling molecules for the formation of biofilms are important virulence factors (3). Thus, these transporters are potential targets for the development of new antimicrobial drugs. As a prerequisite, a detailed understanding at the molecular level of the mechanism by which ABC importers exert their functions is of utmost importance. Structural and biochemical data suggest that alternating access of the translocation pore to the intra- and extracellular space achieves a net transport of substrate. The "leitmotiv" of this model is that the alternation of the TMDs between an outward-facing and an inward-facing conformation is energized by the catalytic cycle of NBDs. The latter includes NBD dimer closure upon ATP binding, hydrolysis of ATP in the closed conformer and reopening toward a semi-closed, ADP-bound state (4). In ABC importers, the interaction of liganded substrate-binding proteins with the TMDs is considered an important step of the transport process.

Because of a plethora of genetic, biochemical, and structural data that have been gathered over more than 3 decades, the enterobacterial maltose transporter MalFGK₂ serves as a model system for studying the mechanism of ABC importers (5, 6). Crystal structures not only exist for three distinct conformations of the isolated NBD dimer MalK₂ (7) but also for MalFGK₂ with bound maltose-binding protein MalE (8). Because of a mutation in MalK, this structure is thought to represent a trapped intermediary state with ATP-bound NBDs. The transmembrane part of the transporter is formed by MalF and MalG. The former includes a large periplasmic domain (MalF-P2)

[1] To whom correspondence may be addressed. Tel.: 49-30-20938121; Fax: 49-30-2093812; E-mail: erwin.schneider@rz.hu-berlin.de.
[2] To whom correspondence may be addressed. Tel.: 41-44-6337570; Fax: 41-44-6331448; E-mail: enrica.bordignon@phys.chem.ethz.ch.

[3] The abbreviations used are: NBD, nucleotide-binding domain; TMD, transmembrane domain; cw, continuous wave; DDM, dodecyl maltoside; TM, transmembrane.

connecting TM helices 3 and 4, which possesses an Ig-like fold and contacts MalE in a cap-like manner in the x-ray structure (Fig. 1). Its function in the catalytic cycle of the transporter is unknown.

In bacterial importers the periplasmic anchoring of the substrate-binding protein is emerging as a key determinant for the nucleotide-induced closure of the cytoplasmically exposed ATP-binding cassette domains of $MalFGK_2$-E (9) and for the transmembrane gates displacement of the vitamin $B_{12}$ importer BtuCD-F (10).

Here we address molecular details of the signaling events occurring on opposite sides of the transporter and present new structural details on the coupling between the periplasmic MalF-P2 and the cytoplasmic MalK dimer in a functional transporter. To this end, we have employed site-directed spin-labeling-electron paramagnetic resonance spectroscopy. A set of interspin distances for five spin-labeled double cysteine mutants in MalF-P2 was obtained by continuous wave (cw) and pulse EPR, thus unveiling mutual rearrangements during the transport cycle. Moreover, concomitant detection of conformational changes in singly spin-labeled $MalK_2$ allowed us to monitor cofactor-induced inter-domain communication. Our study revealed first that MalE binding to MalF-P2 occurs independently of nucleotide binding to $MalK_2$. Second, we could demonstrate a sequence of three conformations of MalF-P2 that corresponds to the nucleotide cycle of the MalK dimer. Finally, we monitored conformational changes simultaneously at the periplasmic and the cytoplasmic faces of the transporter, revealing reciprocal communication between the two domains as a major functional step of the transport process. The correlation of events occurring at both faces of the membrane was shown to be of different robustness with respect to the environment. Based on our results, we propose a model for coupling of ATP hydrolysis and substrate translocation in the maltose transporter.

## EXPERIMENTAL PROCEDURES

*Gene Expression, Protein Preparations, and Spin Labeling*—Cell growth, membrane preparation, and purification of histidine-tagged complexes were performed as described by Landmesser *et al.* (11), except for omitting $MgCl_2$ in the buffer. $His_6$-MalE was purified according to Ref. 12. MalF*G*K2 complexes (where * denotes Cys-less background) were labeled with 2-fold (double cysteine mutants in MalF-P2), 3-fold (MalF*G*K-$(C40S/S83C)_2$), or 5-fold (MalF*(S205C/S252C)G*K(C40S/$S83C)_2$) molar excess of methanethiosulfonate spin label (Alexis Corp., Lauden, Switzerland) for 1 h at 4 °C. Residual methanethiosulfonate spin label was removed by gel filtration (PD-10 columns, GE Healthcare). Spin labeling and measurements were performed in the same buffer used for purification (50 mM Tris-HCl, pH 8.0, 0.01% $\beta$-dodecyl maltoside, 20% (v/v) glycerol). Deuterated glycerol was used in some cases to optimize the signal to noise ratio of the DEER traces. Samples were concentrated using Vivaspin 100 centrifuge filters (Sartorius, Goettingen, Germany) to achieve final concentrations of 100–200 $\mu$M. Cofactors were added before shock-freezing the sample in the quartz tube. Nucleotide binding of the complex was achieved by incubating the sample with 4 mM ATP, 0.1 mM

EDTA or 4 mM ADP and 4 mM $MgCl_2$ (10 min of incubation at room temperature). Post-hydrolytic conformations were obtained by incubation of the sample with 4 mM ATP/4 mM $MgCl_2$ for 20' at 37 °C. MalE was added in double molar excess to the transporter in the presence of 2 mM maltose (10' incubation at room temperature).

*Reconstitution of Spin-labeled $MalFGK_2$ Complexes*—For ATPase activity measurements and distance measurements, spin-labeled maltose transporter variants were reconstituted into liposomes at a 5:1 lipid to protein ratio (*Escherichia coli* polar extract, Avanti Polar Lipids, Alabaster, AL). Reconstitution using Bio-Beads (Bio-Rad) was performed overnight at 4 °C in the presence and absence of liganded MalE. Proteoliposomes where then spun down at 200,000 × $g$ for 1 h at 4 °C, resuspended in the least possible volume of 50 mM Tris-HCl, pH 7.2, flash-frozen in liquid nitrogen, and stored at −80 °C until use.

*ATPase Measurements of Spin-labeled $MalFGK_2$ Variants*—Activity measurements of spin-labeled transport complexes were performed according to Ref. 11. Complexes were assayed both in detergent solution and reconstituted both in the presence and absence of MalE.

*Continuous Wave EPR Measurements*—EPR spectra were recorded at X-band frequencies (9.3–9.4 GHz) with a Bruker Elexsys 580 spectrometer equipped with a Bruker super-high Q cavity and a continuous flow $N_2$ cryostat. For room temperature and 160 K measurements, the microwave power was set to 0.6 and 0.03 milliwatts and the *B*-field modulation amplitude to 0.1 and 0.25 millitesla, respectively. Fitting of simulated dipolar broadened EPR powder spectra to the experimental ones detected at 160 K was performed according to Refs. 13, 14.

*Pulsed EPR Measurements and Data Analysis*—Dipolar time evolution data were obtained at X-band frequencies with a Bruker Elexsys 580 spectrometer equipped with a Bruker Flexline split-ring resonator ER 4118X-MS3 and a continuous flow helium cryostat ESR900 (Oxford Instruments, Oxfordshire, UK) controlled by an Oxford Instruments temperature controller ITC 503S. All measurements were performed as described previously (13) using the four-pulse DEER experiment (15). Experimental data were collected at 50 K with observer pulse lengths of 16 ns for $\pi/2$ and 32 ns for $\pi$ pulses, with the electron double resonance $\pi$ pulse set to 12 ns. Proton or deuterium modulations were averaged. Data analysis of the DEER traces was performed with the software DeerAnalysis 2008.1 (16). All results were found to be independent from the order of added cofactors, and the DEER traces were recorded at least twice from distinct protein preparations.

## RESULTS

*Experimental System*—Fig. 1 shows the sites of introduction of the spin labels in the structure of the maltose ABC importer (Protein Data Bank code 2R6G). Sites 205, 239, and 252 are located in the core of the MalF-P2 loop and were used to measure a triangular pattern of distances to monitor major conformational changes. Sites 92 and 273 are in the regions anchoring MalF-P2 to helices TM3 and TM4, respectively, and were chosen to detect eventual MalF-P2 movements with respect to the membrane plane. To simultaneously detect closure and open-
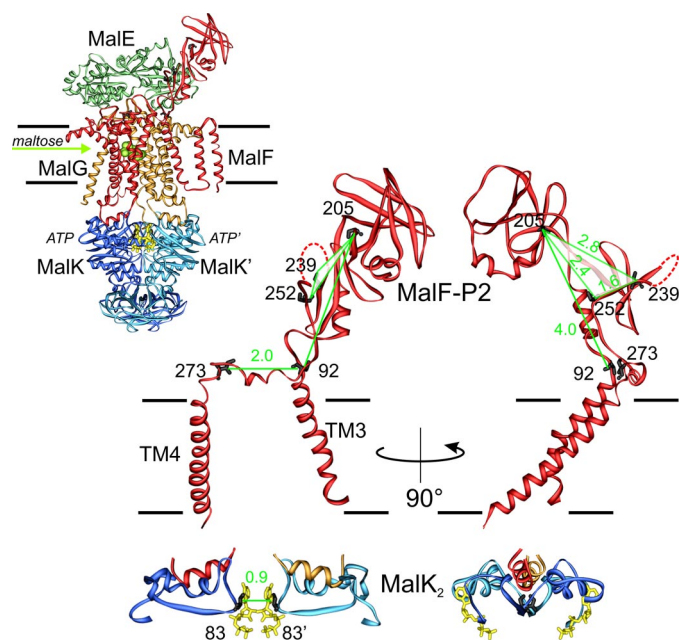
FIGURE 1. **Spin-labeled sites in MalF-P2 and MalK$_2$ in the crystal structure (2R6G).** Maltose and ATP molecules are depicted in *green* and *yellow*, respectively. On the *right*, selected regions of MalF and MalK are highlighted, with the pattern of distances investigated (*green lines*). The MalF (*red*) and MalG (*orange*) coupling helices and the two ATP molecules (*yellow*) are also depicted. The *inset* indicates the C$\beta$-C$\beta$ distances between the side chains in the crystal are depicted in *green*.



FIGURE 2. **Effect of ATP or liganded MalE on the MalF-P2 conformation.** *Left panel,* DEER data F($t$), corrected for an exponentially decaying background arising from a three-dimensional distribution of remote spins. *Right panel,* corresponding distance distributions P($r$) obtained with Tikhonov regularization by DeerAnalysis 2008. *Arrows* indicate changes in F($t$) and in P($r$) induced by liganded MalE (MalE/maltose). For selected mutants, room temperature cw EPR spectra are depicted in the *insets.*

ing of the nucleotide-binding interface and the MalF-P2 rearrangements in the intact transporter, two spin labels were introduced in MalK$_2$ at positions 83/83′ in combination with MalF-P2 sites 205 and 252. All spin-labeled variants of MalFGK$_2$ displayed MalE/maltose-stimulated ATPase activity both in detergent solution and proteoliposomes. However, in some cases, labeling caused a reduction in activity (see supplemental Table S1). Although MalE-independent activity was generally low in proteoliposomes (10% or less), the same complexes exhibited elevated values in detergent solution.

*MalK$_2$ ATP Hydrolysis Cycle Does Not Induce MalF-P2 Loop Rearrangements in the Absence of MalE*—As demonstrated in an earlier EPR study (13), ATP binding and hydrolysis by the complex solubilized in dodecyl maltoside (DDM) induced conformational changes in the MalK dimer in the absence of MalE. Thus, we examined possible effects of the MalK nucleotide cycle on MalF-P2 under the same conditions. Fig. 2 shows the pulse EPR data and selected cw EPR spectra detected for five doubly spin-labeled variants. We found that binding of ATP to MalK$_2$ as well as subsequent hydrolysis failed to induce conformational changes in the core of the MalF-P2 domain (sites 205, 239, and 252). A bimodal distance distribution obtained for all doubly spin-labeled mutants sharing site 239 points to a certain degree of flexibility around this position in the absence of MalE.

No evidence for ATP-induced dislocation of the P2 domain from the adjacent N-terminal transmembrane segment was found, as judged from the invariant distance between site 92 in helix TM3 and 205 in the P2 loop. On the other hand, small spectral changes were detected at room temperature for the 92/273 mutant indicating that nucleotide binding affects the dynamics of the periplasmically exposed face of the transmem-
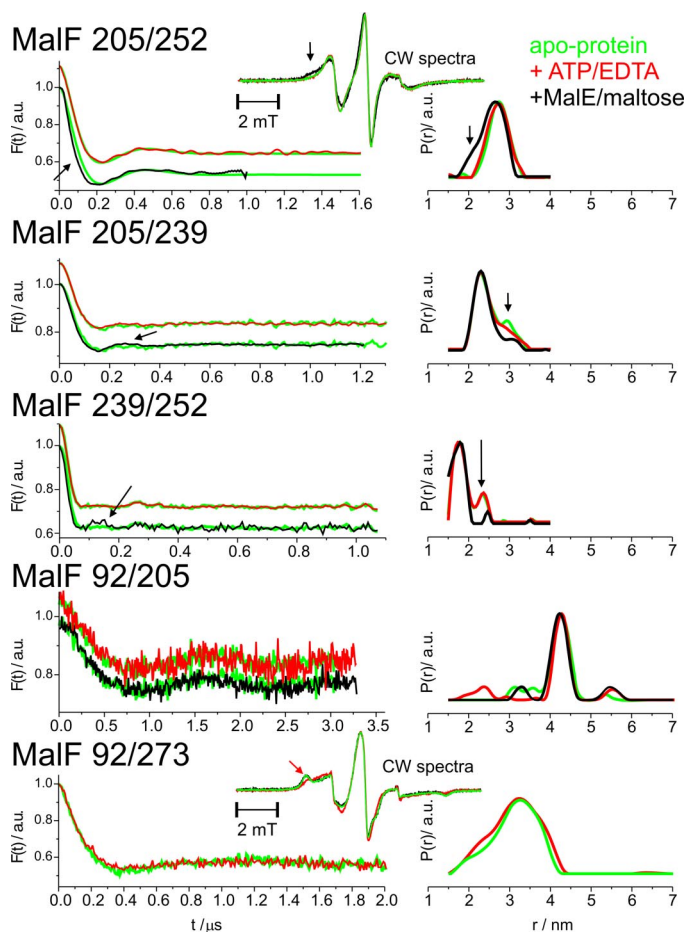
brane domains. The broad interspin distance distribution and the low degree of reproducibility of the DEER traces for the 92/273 mutant indicate that residue 273 is located in a disordered region of the protein, contrary to what was expected from the x-ray data (see also supplemental Fig. S3).

Addition of liganded MalE to the DDM-solubilized complex led to detectable changes in the MalF-P2 core (Fig. 2, *first three panels*). Changes both in spin label dynamics and in interspin distances are indicative for MalE binding to the apo complex. Hence, MalE is sufficient to trigger conformational changes in MalF-P2 even in the absence of ATP. The transition from bimodal to unimodal distance distributions for the doubly spin-labeled mutants sharing position 239 indicates that this region of the MalF-P2 domain is stabilized by MalE.

*Three Distinct Conformations of MalF-P2*—In the presence of liganded MalE, MalF-P2 undergoes relevant conformational changes. In fact, upon ATP binding, we detected distinct interspin distance changes (Fig. 3) ranging from a 0.1 nm increase between 205–239 and 239–252 to a 1.2 nm decrease between sites 205 and 252. Addition of ADP-Mg$^{2+}$ or incubation in the presence of ATP-Mg$^{2+}$ induced an identical distance distribution assigned to the post-hydrolytic state as shown for the 205/
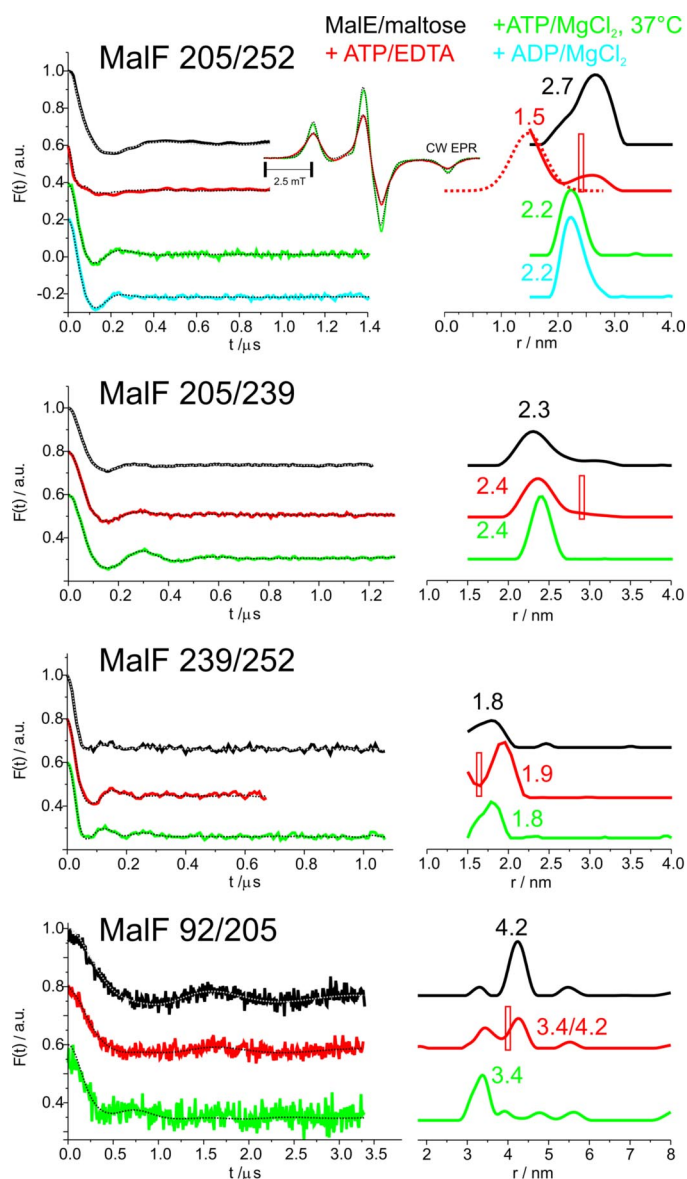
FIGURE 3. **Combined effect of MalE/maltose and nucleotides on the MalF-P2 conformation.** The data in the absence of nucleotides are those already presented in Fig. 2. *Left panel,* DEER data $F(t)$, corrected for an exponentially decaying background arising from a three-dimensional distribution of remote spins. *Right panel,* corresponding distance distributions $P(r)$. For 239/252 Tikhonov regularization parameters 0.1 or 1 were used in combination with the excitation bandwidth correction tool from DeerAnalysis 2008; the small feature around 1.5 nm is noise-related (supplemental Fig. S4). The *red vertical bars* represent the C$\beta$-C$\beta$ distances depicted in Fig. 1 (see also supplemental Fig. S3). The low temperature spin normalized cw EPR spectra detected for 205/252 in the ATP- and ADP-bound states are presented in the *inset*. The simulations (*dotted lines*) revealed a Gaussian distance distribution centered at 1.5 nm for the ATP-bound state, which is superimposed to the DEER-derived distribution in the *right panel* (*red dotted line*).

252 mutant (Fig. 3 and supplemental Fig. S1). Interestingly, the most relevant changes in the post-hydrolytic conformation with respect to the apo-state were found for 92/205 ($-0.8$ nm) and 205/252 ($-0.5$ nm) (Fig. 3).

To correlate the EPR findings with the available x-ray data (8), an inactive transporter variant containing the E159Q mutation in MalK was spin-labeled at positions 205 and 252. This exchange is known to abolish ATP hydrolysis (17). Indeed, the MalF-P2 conformations of the apo- and ATP-bound states in the inactive transporter were indistinguishable from those obtained with the active construct, whereas conditions favoring ATP hydrolysis did not induce the post-hydrolytic conformation. In contrast, direct binding of ADP and MgCl$_2$ to MalK$_2$ was sufficient to trigger the post-hydrolytic MalF-P2 conformation (supplemental Fig. S2). Hence, the transition from the ATP-bound to the post-hydrolytic MalF-P2 conformation is clearly blocked in the inactive E159Q transporter, thus unveiling the reciprocal communication across the membrane between the semi-open conformation of MalK$_2$ and the post-hydrolytic conformation of MalF-P2.

Based on these facts, we surmise that the x-ray structure of MalF-P2 can be compared with the ATP-bound conformation of MalF-P2 in the wild type transporter. The correlation between EPR-derived and x-ray C$\beta$-C$\beta$ distances are presented in Fig. 3 and can be considered as an agreement taking into account the spin label average length (18). Simulations performed on *in silico* labeled residues in MalF-P2 reveal a good qualitative agreement with the experimentally determined interspin distances, despite the generally high *B*-factors of the residues surrounding the spin labels (2R6G). The most relevant deviations were found for the mutant 239/252, with both spin labels close to the 243–244 missing residues in the structure, and for the 92/273 pair, where the EPR data clearly suggest a disordered region around position 273 (supplemental Fig. S3).

*Reconstitution into Liposomes, Effects on NBDs Closure, and Inter-domain Communication*—Results on MalFGK$_2$ spin-labeled at positions 205 and 252 reconstituted into liposomes resemble those obtained in detergent solution (Fig. 4A), indicating that the three observed conformations of MalF-P2 are representative for transporters in a physiological environment.

It is worth mentioning that in the ATP-bound and post-hydrolysis states, a residual peak centered at 2.7 nm and corresponding to 50% of the total area was found (Fig. 4A). This apo state-like peak reflects the fraction of transporters still in the apo state in which the nucleotide binding domains face the lumen and hence remain unaffected by nucleotide addition (11).

Effects of liganded MalE on MalK dimer closure were analogously investigated in the reconstituted complex carrying the spin label at Cys-83 in MalK$_2$. In the absence of MalE, ATP binding induced only a minor distance decrease between the two MalK subunits, even smaller than that found in DDM solution (13). This correlates to the strongly suppressed ATP hydrolysis rate (supplemental Table ST1). In contrast, addition of liganded MalE and ATP induced a tighter closure of the NBDs both in reconstituted and in DDM-solubilized complexes (Fig. 4B). A line shape analysis was performed on the cw EPR spectra of the DDM-solubilized transporters. The mean interspin distance of 1.5 nm was found in agreement with the short distances detected by DEER in proteoliposomes.

A "triple mutant" spin-labeled both in MalK$_2$ (sites 83/83') and in MalF-P2 (sites 205 and 252) and reconstituted in liposomes showed broad DEER traces as expected (Fig. 4C). In the absence of liganded MalE, only minor changes were detected upon ATP binding. The presence of MalE/maltose (in the lumen of the proteoliposomes) induced a pronounced short distance peak indicative of a tighter NBD closure and a conformational switch in the P2 domain (supplemental Fig. S5).
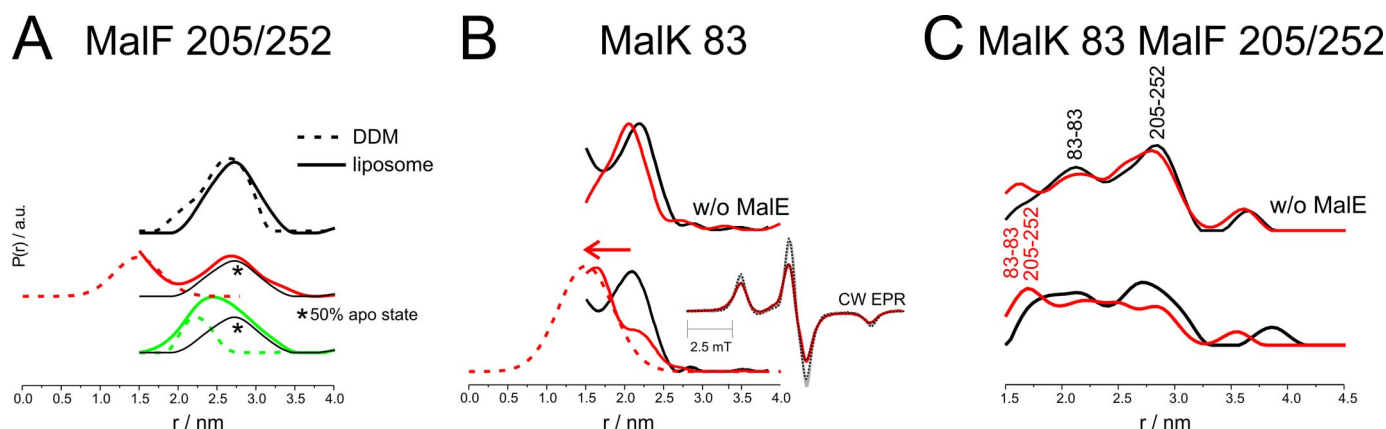
FIGURE 4. **Reciprocal communication in the reconstituted maltose transporter in the presence of MalE/maltose.** Distance distributions *P*(*r*) obtained by DEER and cw EPR. Color code is as follows: apo, *black*; ATP/EDTA, *red*; ATP/MgCl₂, *green*. Data are recorded in the presence of MalE/maltose in the liposome lumen if not otherwise stated. *A,* three MalF-P2 conformations in proteoliposomes detected with MalF 205/252. The residual peak intensity centered at 2.7 nm in the ATP-bound and post-hydrolysis states corresponds to 50% of the total area and clearly reflects the percentage of transporters still in the apo state in which the nucleotide-binding domains face the lumen. The same effect is expected to influence the distance distribution in the ATP-bound state for position 83 and for the triple mutant. *B,* effect of MalE/maltose on NBDs closure detected with MalK 83. The low temperature spin normalized cw EPR spectrum of MalK 83 in DDM micelles in the presence of ATP and MalE/maltose is shown on the *right*. For comparison the reference spectrum without dipolar broadening is superimposed (MalF 205/252, ADP-bound state; see Fig. 3). The calculated Gaussian distance distribution centered at 1.5 nm (*red dashed line*) is superimposed to those obtained by DEER in proteoliposomes. *C,* triple mutant in the apo- and ATP-bound states. The expected distances for MalF 205/252 and MalK₂ 83/83′ in the apo- and ATP-bound states are depicted. All *F*(*t*) traces are presented in supplemental Fig. S5.
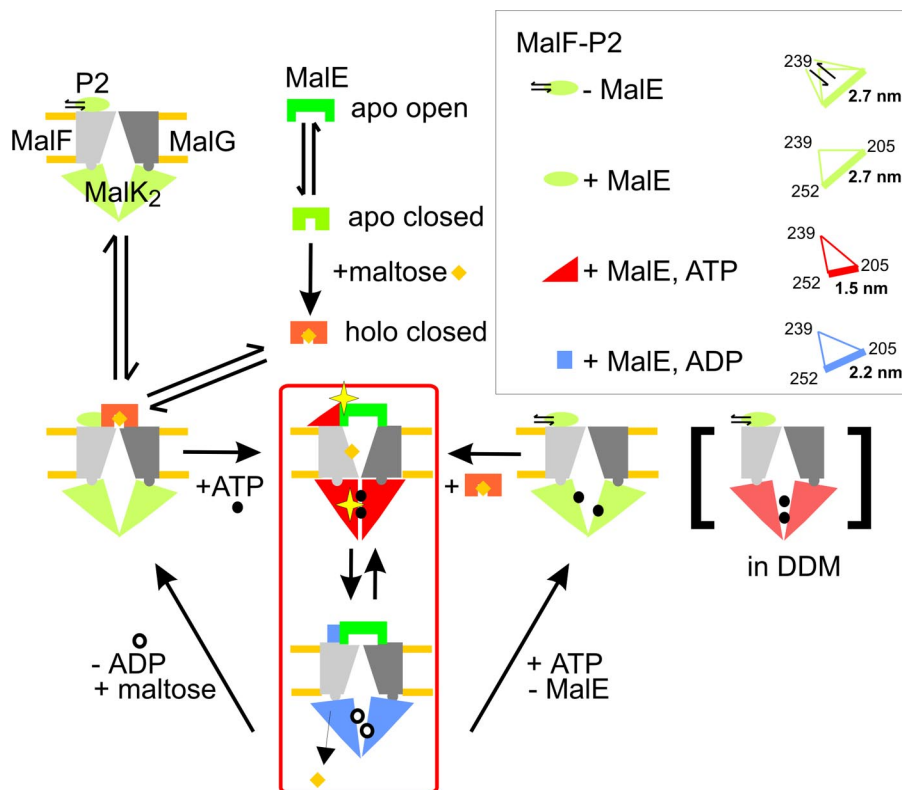


FIGURE 5. **Model for ATP-dependent maltose uptake in MalFGK₂.** Correspondence of three different states detected both in NBDs MalK2 and MalF-P2 is indicated by color coding. TMDs interchange between cytoplasmic and periplasmic open states. An open apo-, a semi-closed apo-, and a closed holo-form of MalE are based on NMR data (24). Transitions between the two conformers highlighted in the *red box* represent ATP-dependent import of maltose. The *stars* denote the unstable nature of the ATP-bound intermediate. The uncoupled state of an ATP-bound transporter in detergent solution is indicated within *square brackets*.

## DISCUSSION

In this study, we analyze conformational changes and inter-subunit communication across the membrane in the maltose ABC transporter by EPR. To this end, transporter variants were spin-labeled both in the cytoplasmically located NBDs (MalK₂)

and in MalF-P2, the large periplasmic domain of MalF. Functional data on this domain are scarce. Insertion or deletion mutations within this region caused maltose-negative phenotypes (19). Daus *et al.* (17) presented first evidence for conformational changes in the MalF-P2 loop during transport. Furthermore, recent biochemical data and an NMR analysis suggested that MalF-P2 is sufficient to bind MalE and stays in intimate contact to the receptor throughout the transport cycle (20, 21).

Our data led to three main conclusions about the catalytic cycle of MalFGK₂. First, binding of MalE to the transporter was demonstrated during the whole nucleotide cycle, with MalE reducing the intrinsic flexibility of MalF-P2 around site 239. Second, a sequence of three distinct MalF-P2 conformers was found analogous to the open, closed, and semi-open conformations of the MalK dimer. Third, and most importantly, we found a reciprocal dependence of conformational changes at the periplasmic and the cytoplasmic face of the transporter, *i.e.* reciprocal communication. Yet the effect of the conformational changes in MalK₂ on MalF-P2 and vice versa is of different robustness with respect to the environment of the transporter. Rearrangements in MalF-P2 are strictly dependent on MalE and ATP both in micelles and membranes. In contrast,

MalK dimer closure despite requiring MalE to be completed (9) can (at least in part) be triggered by ATP alone in detergent solution. This results in a futile ATP hydrolysis cycle unable to trigger the MalF-P2 conformational changes.

The decoupling between MalF-P2 and MalK observed in DDM-solubilized complexes is suggested to be related to an enhanced flexibility of the TMDs in detergent micelles. These findings correspond very well to the elevated levels of MalE-independent ATPase activity that we observed in detergent solution (supplemental Table S1).

Our results give first structural insights into the stimulatory effect of MalE on the ATPase activity. MalE binding is found to be correlated to structural rearrangements in MalF-P2, which need to be transferred through the TMDs to the cytoplasmic coupling helices to trigger the complete closure of the NBDs. Combining our findings with other structural and biochemical data, we present a dynamic model for the coupling of ATP hydrolysis and substrate transfer in $MalFGK_2$ (Fig. 5). According to this model, the transporter is present in an equilibrium of conformers, which is modulated by the concentrations of cofactors and interaction partners. Net transport of substrate is achieved by fine-tuning of the transition rates between the different conformational states. The main features of our model are as follows: (i) the general alternating access principle implying two different conformations of the TMDs (22); (ii) the persistent interaction of liganded MalE with the apo-, ATP-, and ADP-bound conformers of $MalFGK_2$; (iii) the existence of three distinct conformers both in MalF-P2 and $MalK_2$; and (iv) the mutual dependence of conformational changes in MalF-P2 and $MalK_2$, leading to a central conformer with closed NBDs and outward-facing TMDs. This intermediate state can presumably be stabilized only by preventing immediate ATP hydrolysis through mutations (8) or absence of the $Mg^{2+}$ cofactor, for example. Otherwise the equilibrium is strongly shifted toward the ADP-bound conformer with semi-open NBDs and TMDs flipped back toward the cytoplasmic open state, thus releasing maltose into the cytoplasm. It is intriguing that three distinct conformers are emerging in MalF-P2 and $MalK_2$ located at the opposite sites of the membrane, whereas a two-step mechanism switching the TMDs from an outward- to an inward-facing conformation is at present the model for transport. Further studies characterizing the inter-domain relationships during substrate transport will be necessary to scrutinize the model and elaborate the details of the conformational changes triggered by the substrate-binding protein. To this end, spin-labeled MalE variants will be also employed and distances relative to singly spin-labeled positions in the P2-loop and key positions in the transmembrane region of the complex will be investigated. With respect to its details, this model naturally represents the specific situation of the maltose transporter.

Yet also in the BtuCD-F complex, which might have a coupling mechanism distinct from that of the maltose and molybdate importers and which lacks a large anchoring loop for BtuF in BtuCD, both receptor and nucleotides are found to be necessary for the conformational changes in the gates (10, 23). Comparative site-directed spin-labeling EPR studies on the effects of MalE or BtuF on both transporters will help to elucidate the mechanism of substrate-induced activation. From our study, a likely unstable intermediate dependent on the simultaneous presence of two cofactors (receptor/substrate and ATP) is emerging as a key feature for the mechanism of import.

## REFERENCES

1. Holland, I. B., Cole, S., Kuchler, K., and Higgins, C. F. (eds) (2003) *ABC Proteins: From Bacteria to Man*, Academic Press, Inc., New York
2. Crosa, J. H., Mey, A. R., and Eayne, S. M. (2004) *Iron Transport in Bacteria*, American Society for Microbiology, Washington, D. C.
3. Waters, C. M., and Bassler, B. L. (2005) *Annu. Rev. Cell Dev. Biol.* **21,** 319–346
4. Oldham, M. L., Davidson, A. L., and Chen, J. (2008) *Curr. Opin. Struct. Biol.* **18,** 726–733
5. Boos, W., and Shuman, H. (1998) *Microbiol. Mol. Biol. Rev.* **62,** 204–229
6. Davidson, A. L., Dassa, E., Orelle, C., and Chen, J. (2008) *Microbiol. Mol. Biol. Rev.* **72,** 317–364
7. Lu, G., Westbrooks, J. M., Davidson, A. L., and Chen, J. (2005) *Proc. Natl. Acad. Sci. U. S. A.* **102,** 17969–17974
8. Oldham, M. L., Khare, D., Quiocho, F. A., Davidson, A. L., and Chen, J. (2007) *Nature* **450,** 515–521
9. Orelle, C., Ayvaz, T., Everly, R. M., Klug, C. S., and Davidson, A. L. (2008) *Proc. Natl. Acad. Sci. U. S. A.* **105,** 12837–12842
10. Goetz, B. A., Perozo, E., and Locher, K. P. (2009) *FEBS Lett.* **583,** 266–270
11. Landmesser, H., Stein, A., Blüschke, B., Brinkmann, M., Hunke, S., and Schneider, E. (2002) *Biochim. Biophys. Acta* **1565,** 64–72
12. Daus, M. L., Berendt, S., Wuttge, S., and Schneider, E. (2007) *Mol. Microbiol.* **66,** 1107–1122
13. Grote, M., Bordignon, E., Polyhach, Y., Jeschke, G., Steinhoff, H. J., and Schneider, E. (2008) *Biophys. J.* **95,** 2924–2938
14. Steinhoff, H. J., Radzwill, N., Thevis, W., Lenz, V., Brandenburg, D., Antson, A., Dodson, G., and Wollmer, A. (1997) *Biophys. J.* **73,** 3287–3298
15. Pannier, M., Veit, S., Godt, A., Jeschke, G., and Spiess, H. W. (2000) *J. Magn. Reson.* **142,** 331–340
16. Jeschke, G., Chechik, V., Ionita, P., Godt, A., Zimmermann, H., Banham, J., Timmel, C. R., Hilger, D., and Jung, H. (2006) *Appl. Magn. Res.* **30,** 473–498
17. Daus, M. L., Landmesser, H., Schlosser, A., Müller, P., Herrmann, A., and Schneider, E. (2006) *J. Biol. Chem.* **281,** 3856–3865
18. Beier, C., and Steinhoff, H. J. (2006) *Biophys. J.* **91,** 2647–2664
19. Tapia, M. I., Mourez, M., Hofnung, M., and Dassa, E. (1999) *J. Bacteriol.* **181,** 2267–2272
20. Daus, M. L., Grote, M., and Schneider, E. (2009) *J. Bacteriol.* **191,** 754–761
21. Jacso, T., Grote, M., Daus, M., Schmieder, P., Keller, S., Schneider, E., and Reif, B. (2009) *Biochemistry* **48,** 2216–2225
22. Dawson, R. J., and Locher, K. P. (2007) *FEBS Lett.* **581,** 935–938
23. Hvorup, R. N., Goetz, B. A., Niederer, M., Hollenstein, K., Perozo, E., and Locher, K. P. (2007) *Science* **317,** 1387–1390
24. Tang, C., Schwieters, C. D., and Clore, G. M. (2007) *Nature* **449,** 1078–1082